Supplementary Information

In situ interphase engineering for all-solid-state Li batteries: A case study on $LiNi_{0.5}Mn_{1.5}O_4/Li_{0.33}La_{0.55}TiO_3$ composite cathode guided with *ab initio* calculations

Che-an Lin[1], Martin Ihrig[2], Kuan-chen Kung[1], Hsiang-ching Chen[1], Martin Finsterbusch[3], Olivier Guillon[3],

and Shih-kang Lin[1, 4, 5, 6]*

[1] Department of Materials Science and Engineering, National Cheng Kung University, Tainan 70101, Taiwan
[2] Department of Chemical Engineering, National Taiwan University of Science and Technology, Taipei 106, Taiwan
[3] Institute of Energy and Climate Research – Materials Synthesis and Processing (IEK-1), Forschungszentrum Jülich GmbH, 52425 Jülich, Germany
[4] Hierarchical Green-Energy Materials (Hi-GEM) Research Center, National Cheng Kung University, Tainan 70101, Taiwan
[5] Program on Smart and Sustainable Manufacturing, Academy of Innovative Semiconductor and Sustainable Manufacturing, National Cheng Kung University, Tainan 70101, Taiwan
[6] Core Facility Center, National Cheng Kung University, Tainan 70101, Taiwan

*Corresponding author: Email: linsk@mail.ncku.edu.tw (S.-k. Lin)

This PDF contains 14 figures, 4 tables, 1 reference, and supplementary texts.

LNMO/LLTO interfacial stability calculation before and after charging

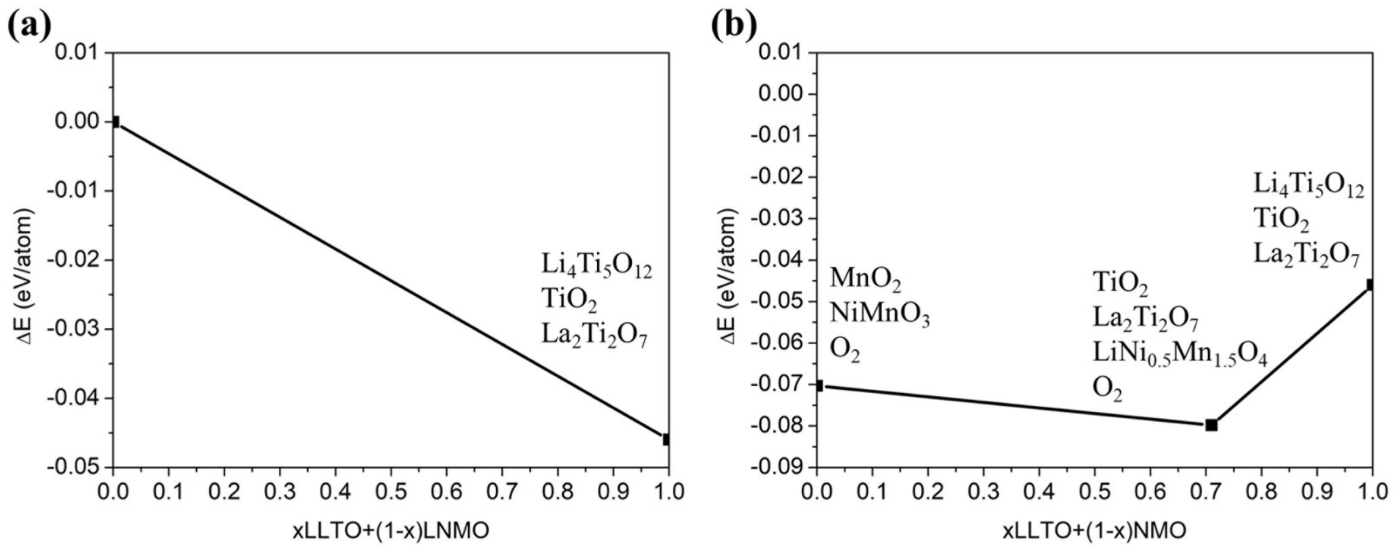

Figure S1. Interfacial convex hulls of (a) $LiNi_{0.5}Mn_{1.5}O_4$ (fully discharged LNMO)/LLTO interface and (b) $Ni_{0.5}Mn_{1.5}O_4$ (fully charged LNMO)/LLTO interface.

LNMO doping stabiltiy computation

To calculate the interfacial reactions between doped LNMO and LLTO, the preferred doping site of each dopant should be obtained. The decomposition energies of main group metals (Na, K, Mg, Ca, Al, Ga, Ge, Sn, Sb), 3d transition metals (Ti, V, Cr, Fe, Co, Cu, Zn), 4d transition metals (Zr, Nb, Mo), and 5d transition metals (W, Ta) doping into the Li, Ni, and Mn sites of disordered LNMO were calculated. As shown in Equation (1), the decomposition energy is the reaction energy of doped LNMO reacting into its competing phases. Unstable dopants with more negative decomposition energies compared to Na substituting Li site were excluded from further computations.[1] By comparing the decomposition energies of dopants in each site, the most preferred doping site of each stable doping system was selected for interfacial reaction calculation, as shown in Table S1.

Table S1. Stable dopants and their preferred doping site in LNMO

Stable dopants	Preferred doping site
Na	Mn site
Mg	Mn site
Al	Mn site
Ca	Mn site
Ga	Mn site
Ge	Ni site
Sn	Ni site
Sb	Ni site
Ti	Ni site
V	Mn site
Cr	Mn site
Fe	Mn site
Co	Mn site
Cu	Mn site
Zn	Mn site
Nb	Ni site
Ru	Ni site
Ta	Ni site
W	Ni site

Mg-, Al-, Sb-, and Cr-doped LNMO/LLTO interfacial convex hulls

$Li_{32}Ni_{16}Mn_{47}MgO_{128}$, $Li_{32}Ni_{16}Mn_{47}AlO_{128}$, $Li_{32}Ni_{15}Mn_{48}SbO_{128}$, or $Li_{32}Ni_{16}Mn_{47}CrO_{128}$ are labeld as Mg-doped LNMO, Al-doped LNMO, Sb-doped LNMO, and Cr-doped LNMO, respectively.

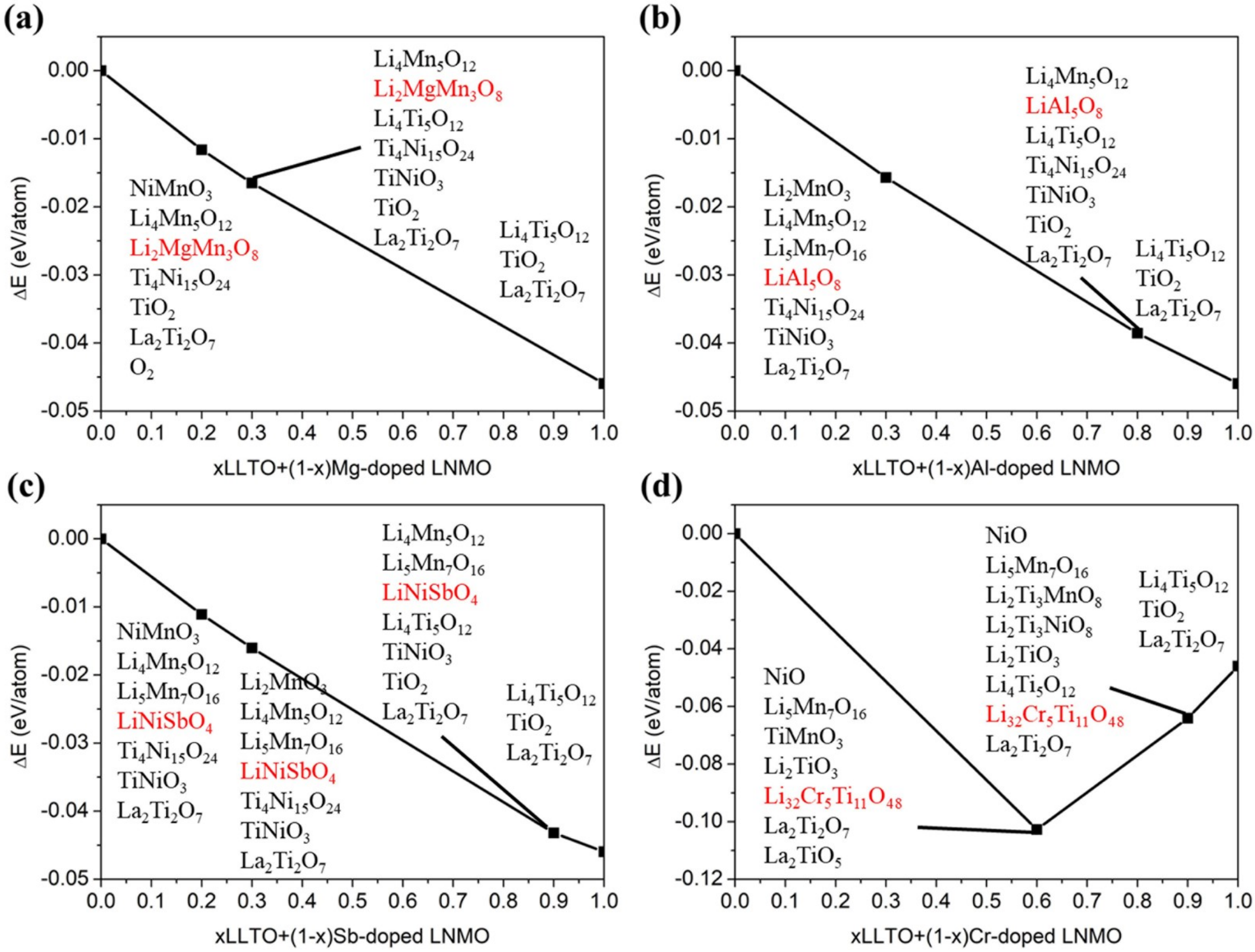

Figure S2. (a) Mg-, (b) Al-, (c) Sb-, and (d) Cr-doped LNMO/LLTO interfacial convex hulls.

Dopant-induced interphases in doped LNMO/LLTO

Table S2. Dopant-induced interphases in doped LNMO/LLTO

Dopant	Dopant-induced interphases
Na	NaO_2, $NaMn_3O_7$
Mg	$Li_2MgMn_3O_8$
Al	$LiAl_5O_8$
Ca	$Ca_2Ti_3O_8$
Ga	Ga_2NiO_4
Ge	Ni_2GeO_4
Sn	SnO_2
Sb	$LiNiSbO_4$
Ti	$TiNiO_3$
V	$LaVO_4$
Cr	$Li_{32}Ti_5Cr_{11}O_{48}$
Fe	La_2FeO_6
Co	CoO
Cu	$LaCu_2O_4$, Cu_2O_3
Zn	$Mn_4Zn_3Ni_2O_{12}$, $ZnNi_2O_4$
Nb	$LaNbO_4$
Ru	La_4RuO_6
Ta	$LaTaO_4$
W	La_2WO_6

Stability of $Li_2MgMn_3O_8$, $LiAl_5O_8$, $LiNiSbO_4$, and $Li_{32}Ti_5Cr_{11}O_{48}$ against fully delithiated LNMO

$Ni_{16}Mn_{47}MgO_{128}$, $Ni_{16}Mn_{47}AlO_{128}$, $Ni_{15}Mn_{48}SbO_{128}$, and $Ni_{16}Mn_{47}CrO_{128}$ are labeled as Mg-doped NMO, Al-doped NMO, Sb-doped NMO, and Cr-doped NMO, respectively.

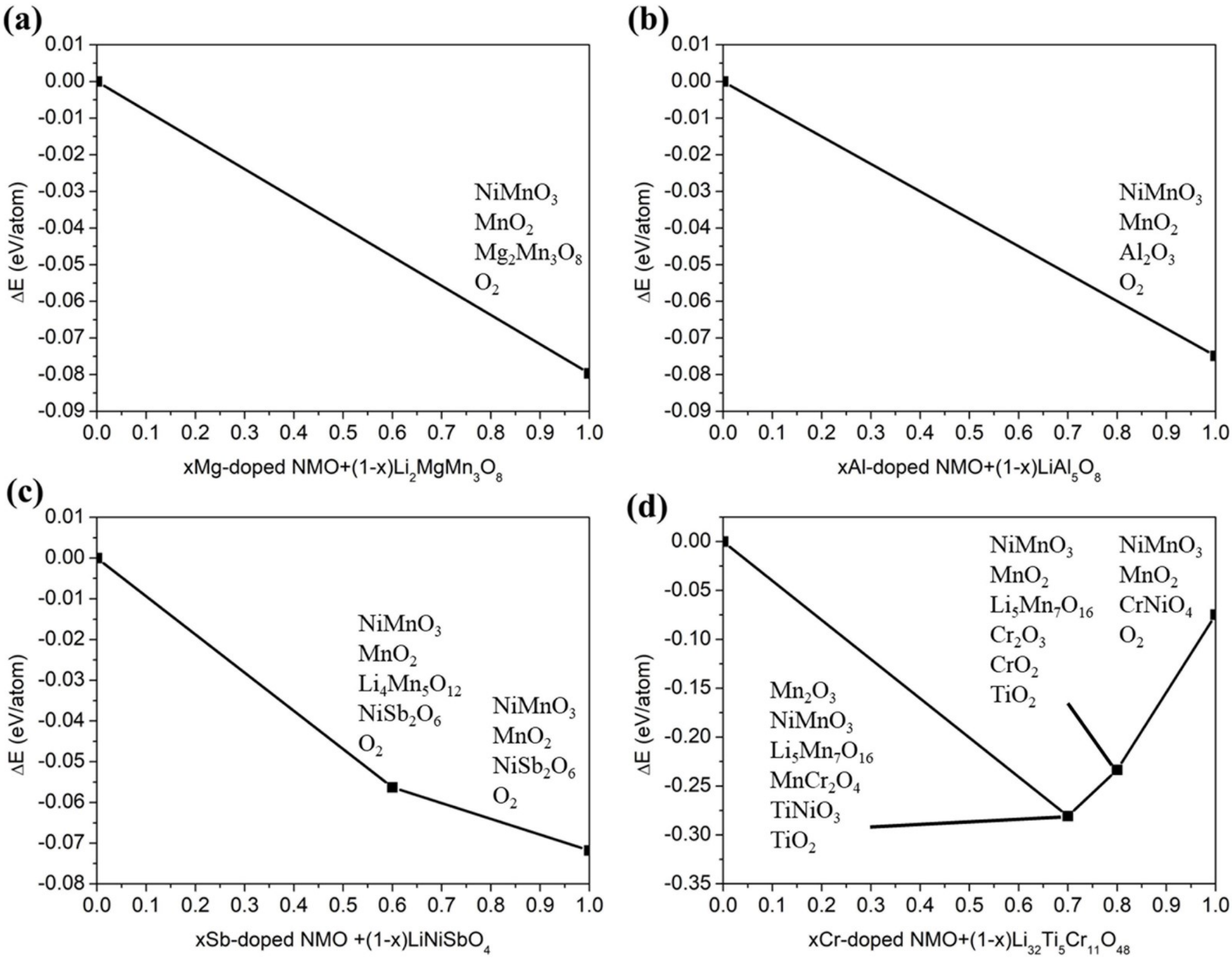

Figure S3. Interfacial sonvex hulls of (a) $Li_2MgMn_3O_8$, (b) $LiAl_5O_8$, (c) $LiNiSbO_4$, and (d) $Li_{32}Ti_5Cr_{11}O_{48}$ against fully delithiated LNMO.

$Li_2MgMn_3O_8$ and $LiAl_5O_8$ density of states

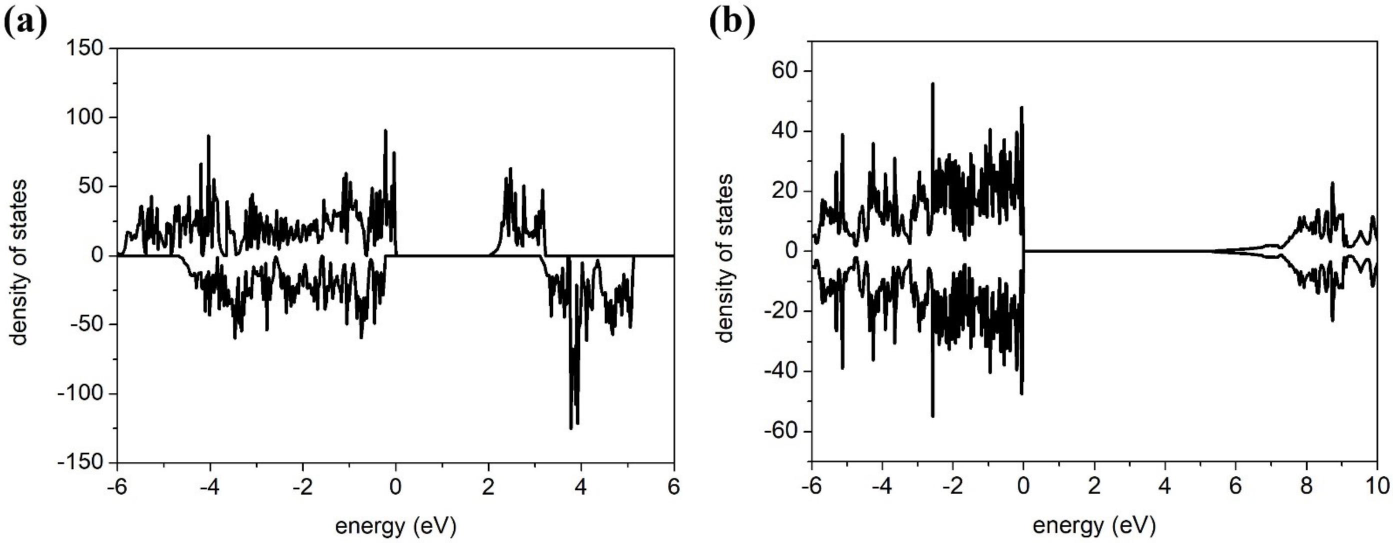

Figure S4. (a) $Li_2MgMn_3O_8$ and (b) $LiAl_5O_8$ density of states.

$LiAl_5O_8$ atomic structure

The red, blue, and green atoms are O, Al, and Li, repectively.

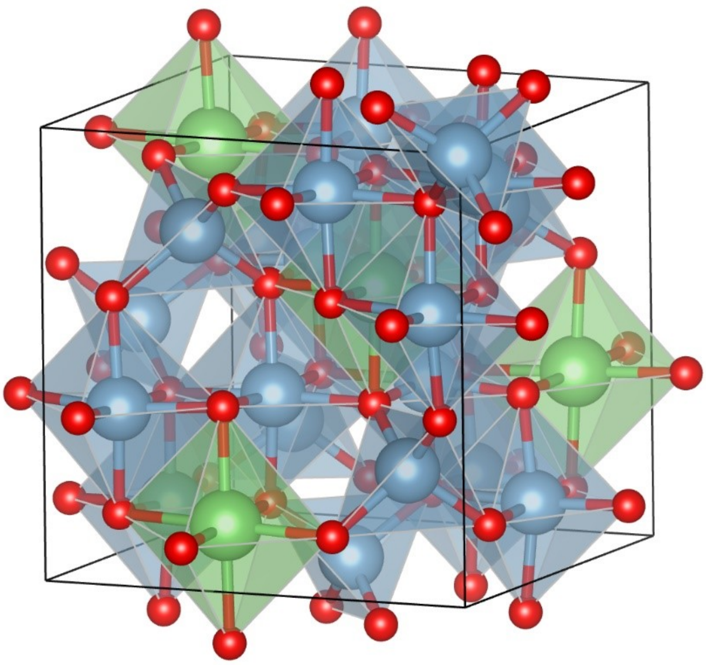

Figure S5. $LiAl_5O_8$ atomic model.

$LiNi_{0.5}Mn_{1.5}O_4$, $LiNi_{0.5}Mn_{1.45}Al_{0.05}O_4$, $LiNi_{0.5}Mn_{1.425}Al_{0.075}O_4$, and $LiNi_{0.5}Mn_{1.4}Al_{0.1}O_4$ XRD analysis

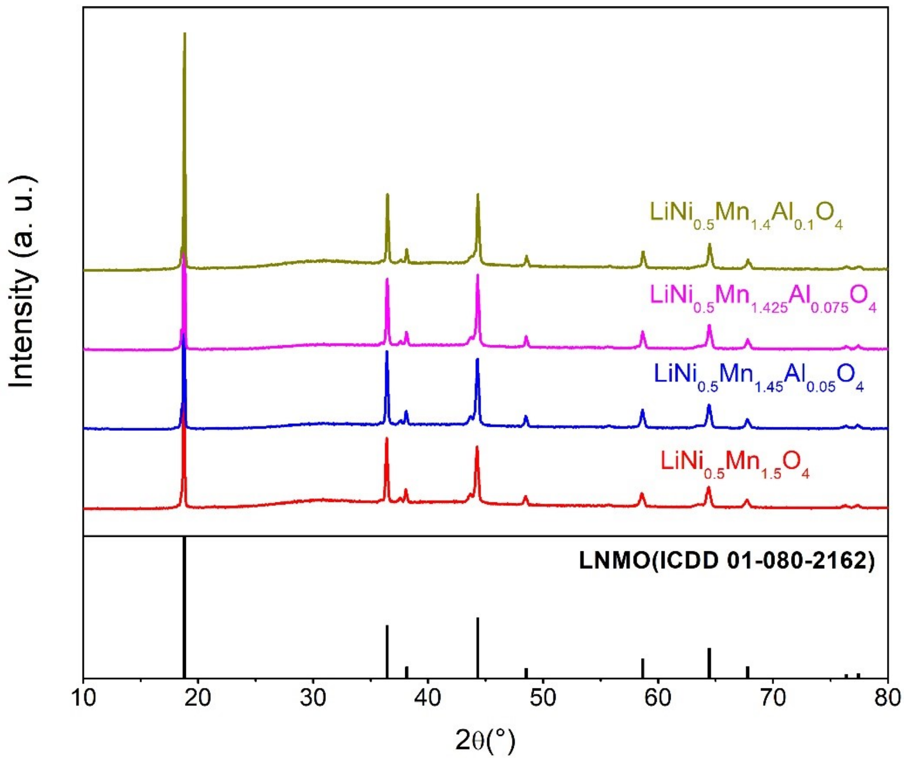

Figure S6. XRD patterns of (a) $LiNi_{0.5}Mn_{1.5}O_4$, (b) $LiNi_{0.5}Mn_{1.45}Al_{0.05}O_4$, (c) $LiNi_{0.5}Mn_{1.425}Al_{0.075}O_4$, and (d) $LiNi_{0.5}Mn_{1.4}Al_{0.1}O_4$.

Dilatometry analysis for LNMO/LLTO and Al-LNMO/LLTO

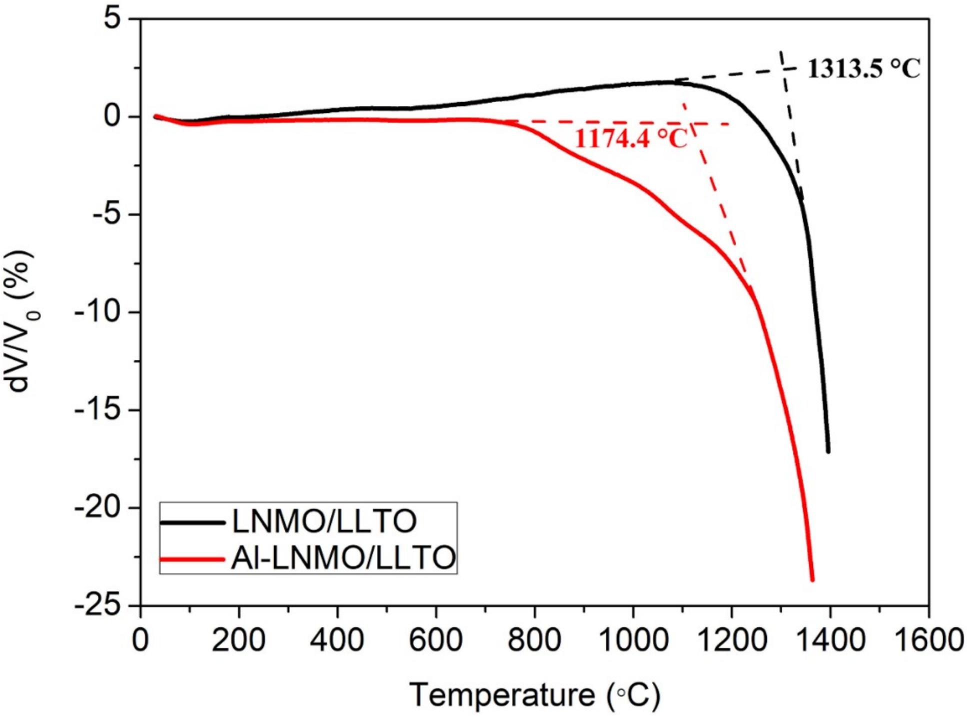

Figure S7. Dilatometry analysis for LNMO/LLTO and Al-LNMO/LLTO mixtures.

DTA and TGA for LNMO and Al-LNMO powders

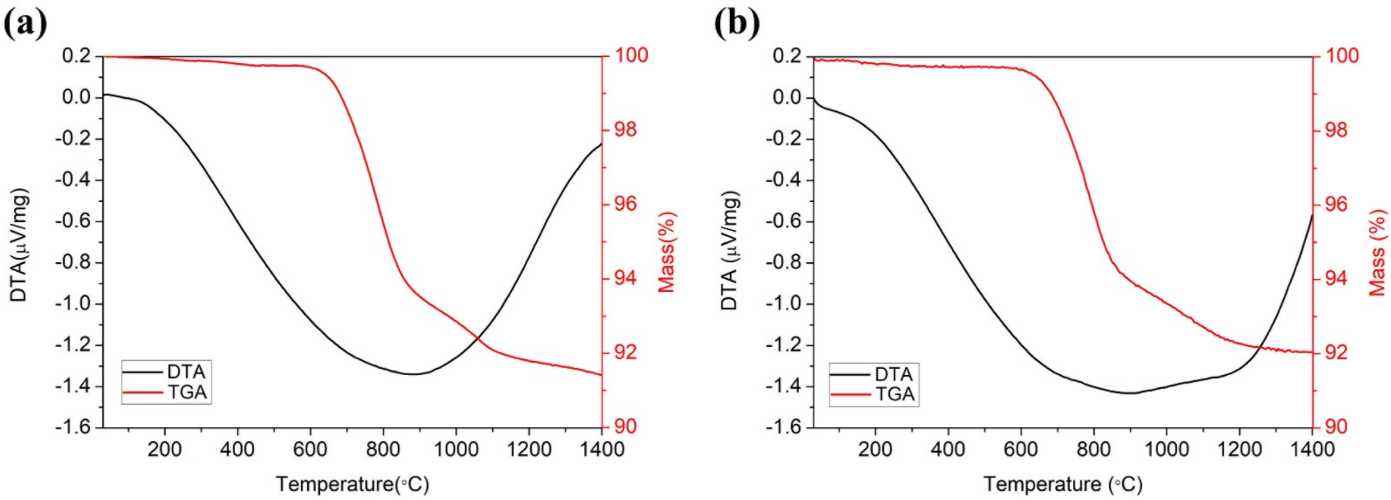

Figure S8. DTA and TGA for (a) LNMO and (b) Al-LNMO powders.

XRD analysis for as-sintered and annealed LNMO/LLTO and Al-LNMO/LLTO composite cathodes

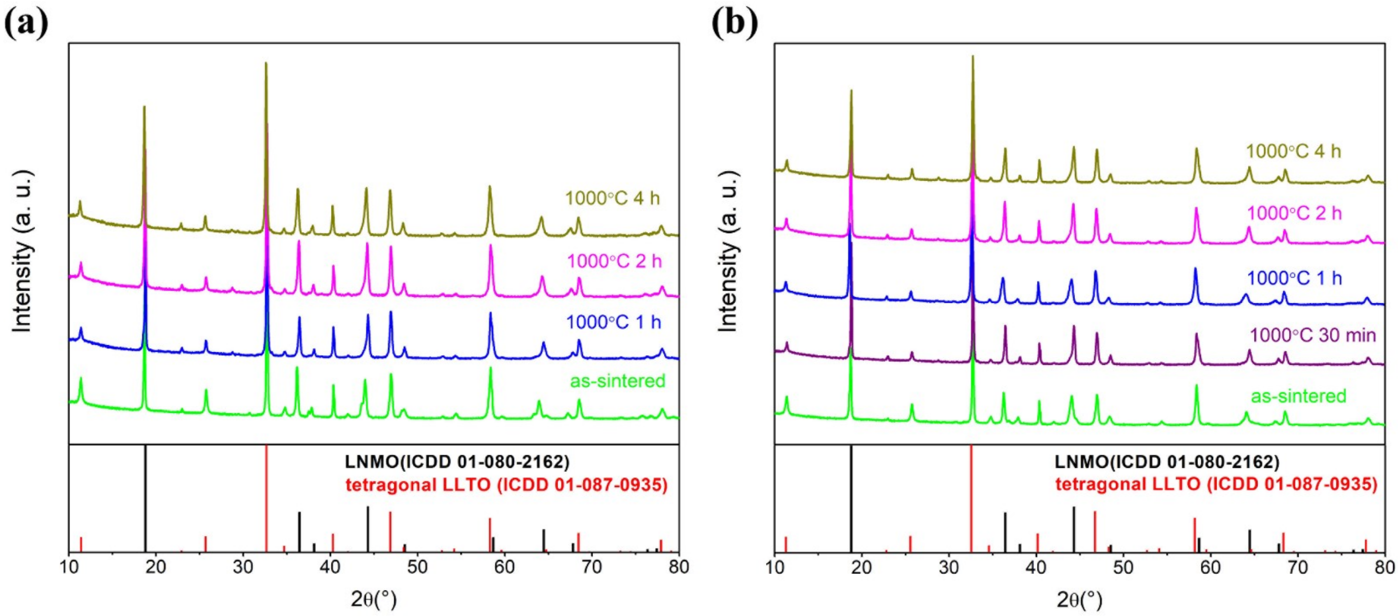

Figure S9. XRD patterns of as-sintered and annealed (a) LNMO/LLTO and (b) Al-LNMO/LLTO composite cathodes.

EDS line profiles of FAST/SPS-sintered, heat-treated, and charged LNMO/LLTO interface

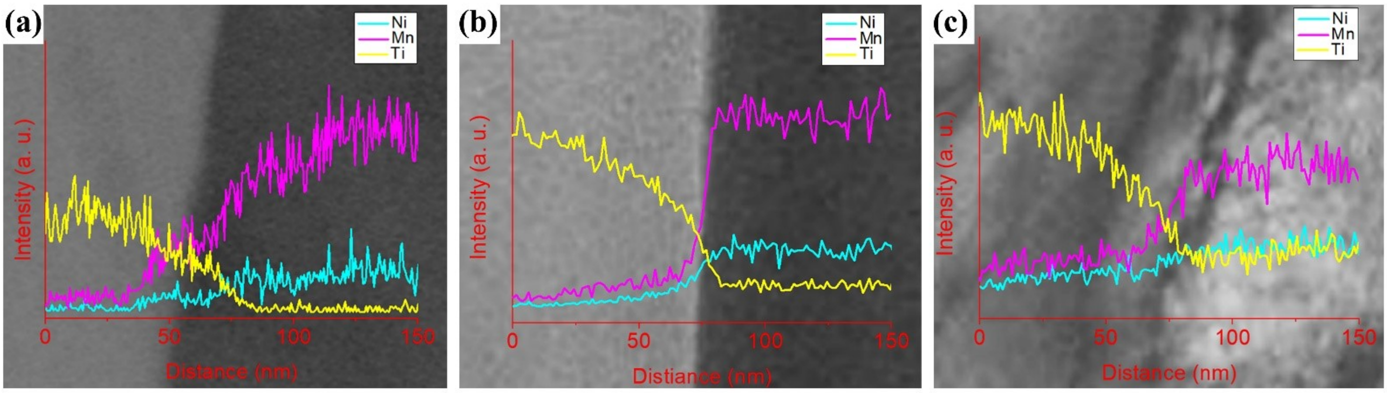

Figure S10. EDS line profiles of (a) FAST/SPS-sintered, (b) 1000 °C 2 h heat-treated, and (c) charged LNMO/LLTO interface.

SAED patterns of FAST/SPS-sintered, heat-treated, and charged LNMO/LLTO

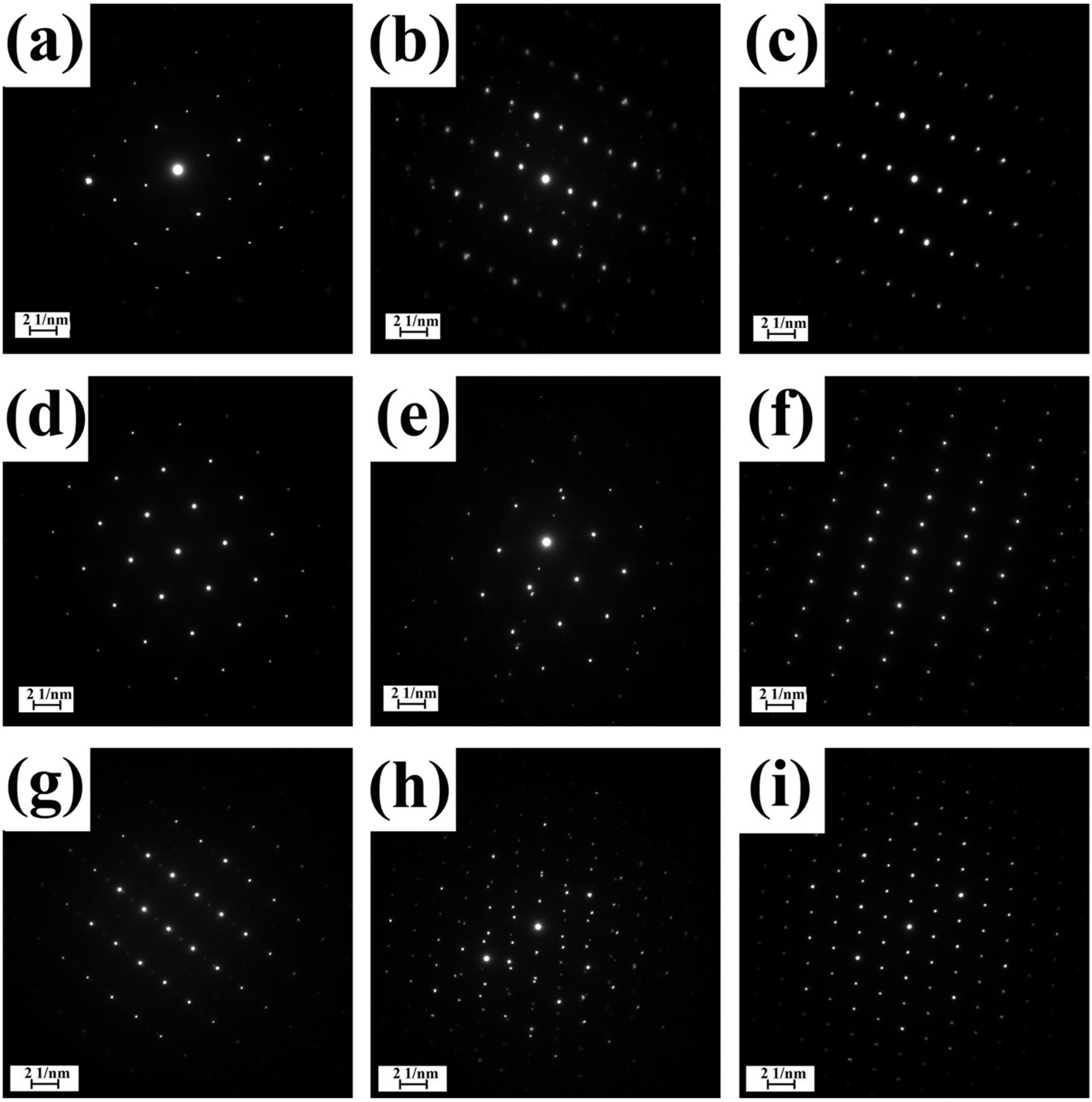

Figure S11. SAED patterns of FAST/SPS-sintered LNMO/LLTO at (a) LLTO, (b) interface, and (c) LNMO, 1000 °C 2 h heat-treated LNMO/LLTO at (d) LLTO, (e) interface, and (f) LNMO, and charged LNMO/LLTO at (g) LLTO, (h) interface, and (i) LNMO.

EDS line profiles of FAST/SPS-sintered, heat treated, and charged Al-LNMO/LLTO interface

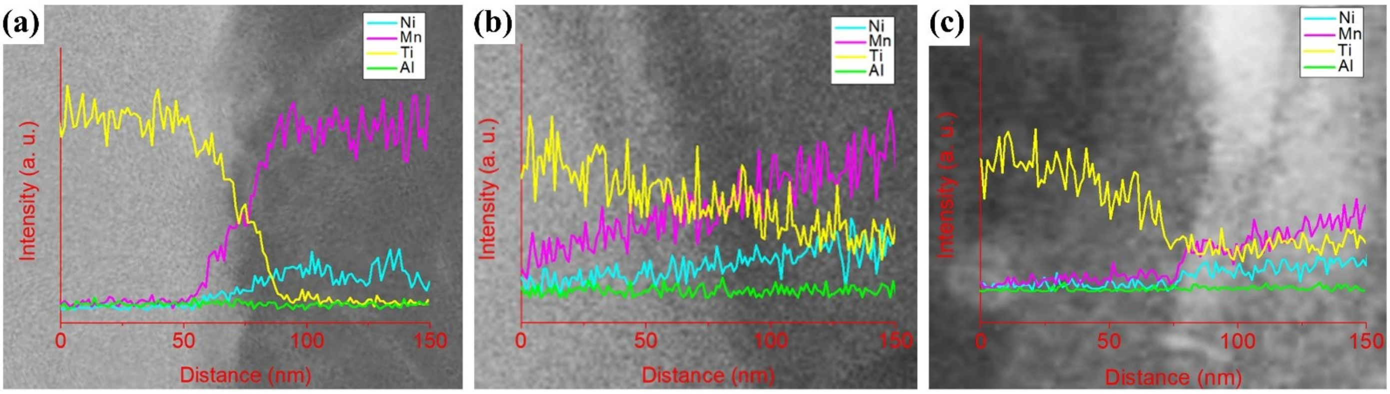

Figure S12. EDS line profiles of (a) FAST/SPS-sintered, (b) 1000 °C 1 h heat-treated, and (c) charged Al-LNMO/LLTO interface.

SAED patterns of FAST/SPS-sintered, heat-treated, and charged Al-LNMO/LLTO

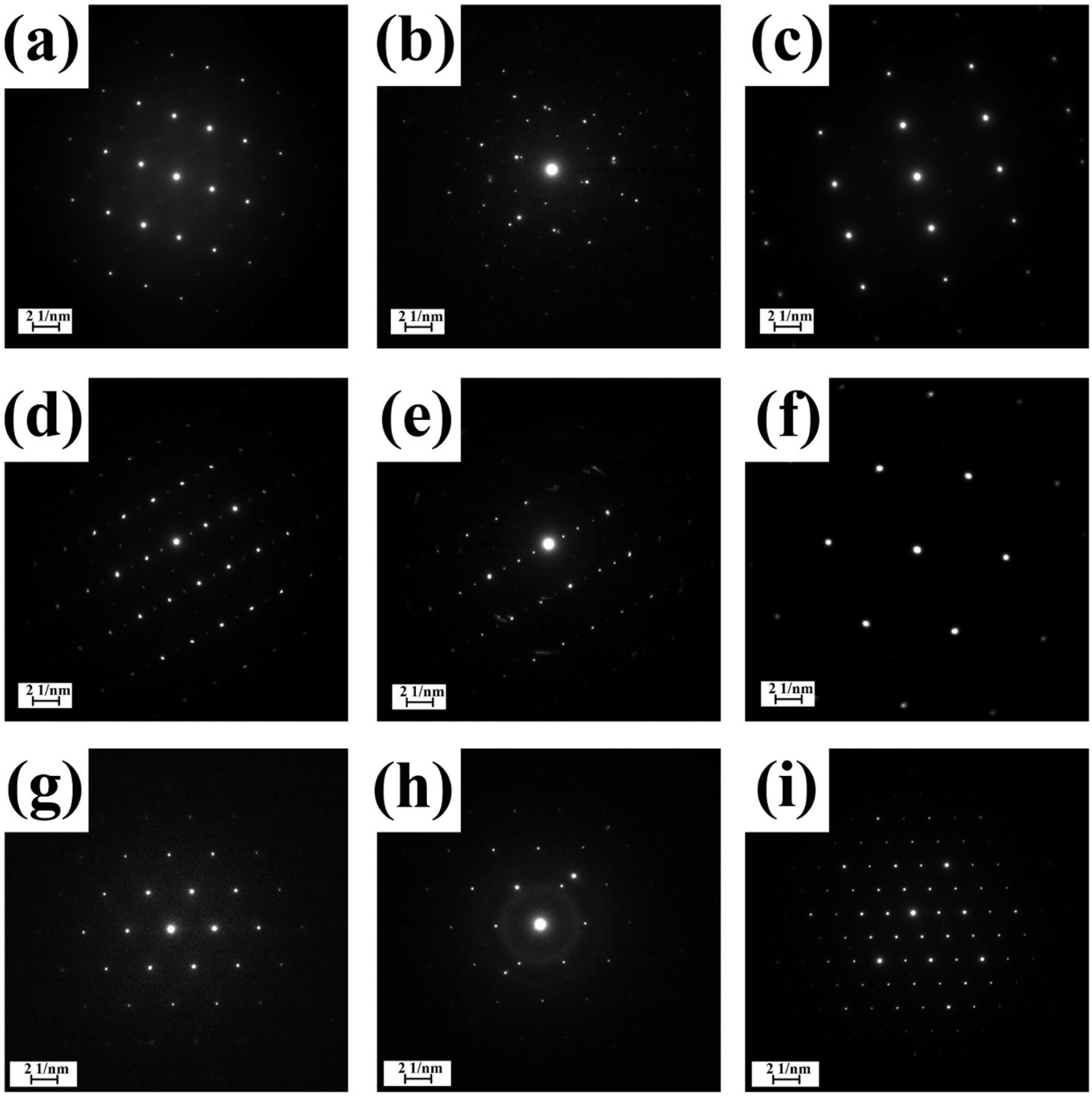

Figure S13. SAED patterns of FAST/SPS-sintered Al-LNMO/LLTO at (a) LLTO, (b) interface, and (c) Al-LNMO, 1000 °C 1 h heat-treated Al-LNMO/LLTO at (d) LLTO, (e) interface, and (f) Al-LNMO, and charged Al-LNMO/LLTO at (g) LLTO, (h) interface, and (i) Al-LNMO.

First-charge curves of LNMO/LLTO and Al-LNMO/LLTO composite cathodes

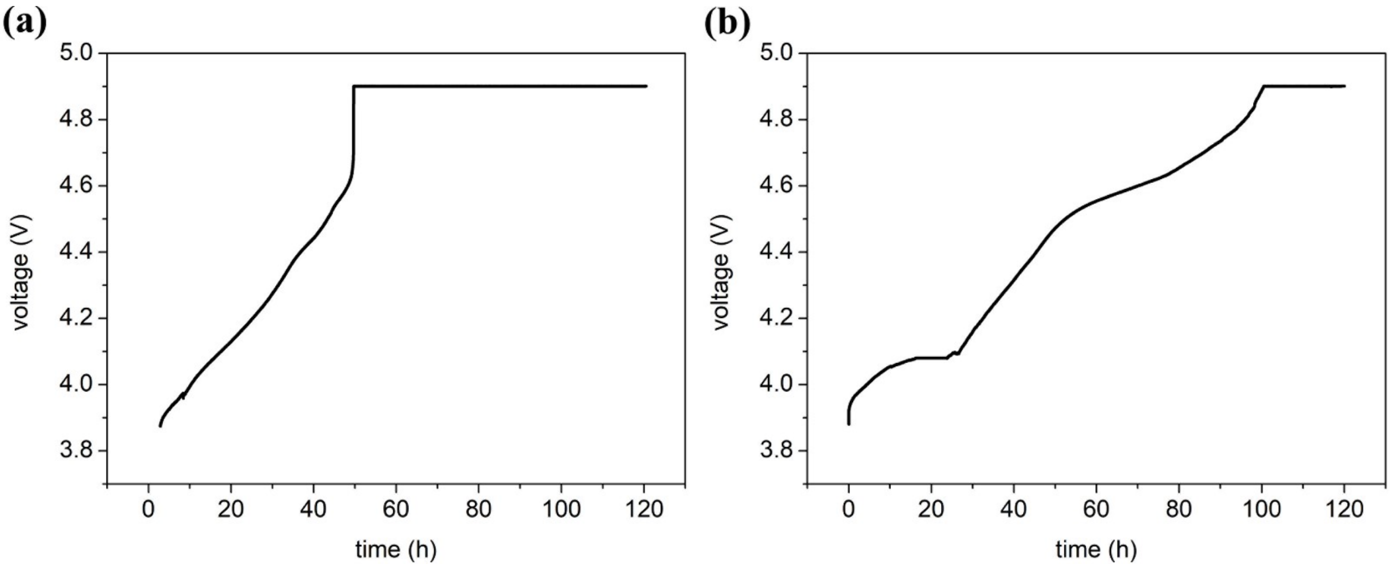

Figure S14. First-charge curves of (a) LNMO/LLTO and (b) Al-LNMO/LLTO composite cathodes.

Fitted impedance values from FAST/SPS-sintered and heat-treated LNMO/LLTO composite cathode

Table S3. Fitted impedance values from FAST/SPS-sintered and heat-treated LNMO/LLTO composite cathode.

	FAST/SPS-sintered	1 h heat-treated	2 h heat-treated	4 h heat-treated
R1 (Ω)	48	41	50	48
Q2 ($F \cdot s^{a-1}$)	3.125E-8	1.5E-9	1.8E-8	3.77E-9
a2	0.7725	0.8626	0.7413	0.8049
R2 (Ω)	131	434	249	273
Q3 ($F \cdot s^{a-1}$)	7.9E-7	5.06E-7	1.84E-6	3.83E-7
a3	0.7713	0.6013	0.5849	0.7035
R3 (Ω)	1709	1163	462	400
Q4 ($F \cdot s^{a-1}$)	3.85E-5	7.53E-6	1.96E-5	2.3E-5
a4	0.393	0.6788	0.7143	0.7521
R4 (Ω)	3545	2763	929	935
Q5 ($F \cdot s^{a-1}$)	8.38E-7	3.6E-6	6.95E-6	1.15E-5
a5	0.6152	0.7449	0.8854	0.8386
R5 (Ω)	1451	814	238	236

Fitted impedance values from FAST/SPS-sintered and heat-treated Al-LNMO/LLTO

Table S4. Fitted impedance values from as-sintered and annealed Al-LNMO/LLTO.

	FAST/SPS-sintered	30 min heat-treated	1 h heat-treated	2 h heat-treated	4 h heat-treated
R1 (Ω)	46	46	48	43	46
Q2 ($F \cdot s^{a-1}$)	1.54E-9	2.91E-9	6.26E-9	1.04E-9	1.12E-9
a2	0.8912	0.821	0.7624	0.8689	0.8667
R2 (Ω)	155	455	452	452	504
Q3 ($F \cdot s^{a-1}$)	6.75E-7	1.06E-6	5.27E-7	5.61E-7	3.69E-7
a3	0.5826	0.5581	0.6687	0.6037	0.6418
R3 (Ω)	1445	1431	491	1059	1062
Q4 ($F \cdot s^{a-1}$)	2.58E-5	7.76E-6	1.09E-5	1.02E-5	1.15E-5
a4	0.4505	0.6366	0.7296	0.7071	0.7422
R4 (Ω)	5918	4037	1341	2136	2109
Q5 ($F \cdot s^{a-1}$)	8.56E-7	4.27E-6	4.33E-6	4.79E-6	6.44E-6
a5	0.6417	0.7239	0.811	0.7902	0.7975
R5 (Ω)	3925	979	391	610	583

Reference

1. Wang, J.; Lin, W.; Wu, B.; Zhao, J., Syntheses and electrochemical properties of the Na-doped $LiNi_{0.5}Mn_{1.5}O_4$ cathode materials for lithium-ion batteries. *Electrochimica Acta* **2014,** *145*, 245-253. https://doi.org/10.1016/j.electacta.2014.07.140